Fishnet Statistical Size Effect on Strength of Materials With Nacreous Microstructure

Wen Luo
Theoretical and Applied Mechanics,
Northwestern University, CEE/A123,
Evanston, IL 60208
e-mail: wenluo2016@u.northwestern.edu

Zdeněk P. Bažant[1]
McCormick Institute Professor,
W.P. Murphy
Professor of Civil and Mechanical
Engineering and Materials Science,
Northwestern University,
Evanston, IL 60208
e-mail: z-bazant@northwestern.edu

The statistical size effect has generally been explained by the weakest-link model, which is valid if the failure of one representative volume element (RVE) of material, corresponding to one link, suffices to cause failure of the whole structure under the controlled load. As shown by the recent formulation of fishnet statistics, this is not the case for some architectured materials, such as nacre, for which one or several microstructural links must fail before reaching the maximum load or the structure strength limit. Such behavior was shown to bring about major safety advantages. Here, we show that it also alters the size effect on the median nominal strength of geometrically scaled rectangular specimens of a diagonally pulled fishnet. To derive the size effect relation, the geometric scaling of a rectangular fishnet is split into separate transverse and longitudinal scalings, for each of which a simple scaling rule for the median strength is established. Proportional combination of both then yields the two-dimensional geometric scaling and its size effect. Furthermore, a method to infer the material failure probability (or strength) distribution from the median size effect obtained from experiments or Monte Carlo simulations is formulated. Compared to the direct estimation of the histogram, which would require more than ten million test repetitions, the size effect method requires only a few (typically about six) tests for each of three or four structure sizes to obtain a tight upper bound on the failure probability distribution. Finally, comparisons of the model predictions and actual histograms are presented. [DOI: 10.1115/1.4043663]

1 Introduction

The amazing mechanical robustness of bioinspired hierarchical materials, such as nacre [1–3], the shell of a conch [4,5], or the exoskeleton of a figeater beetle [6], has been extensively studied over the past two decades. Understanding of the deterministic toughening mechanism and of the critical role of the hierarchical fine-scale structure in enhancing material toughness has been achieved and fostered the advent of novel bioinspired materials [7–9]. However, the stochastic aspects of these hierarchical materials and their effects on the mechanical behavior have received relatively little attention. Nukala and Simunovic [10] simulated the process of random fracturing of nacre by the random fuse model. Recently, Abid et al. [11] modeled the fracturing process using the discrete element method with randomized material properties. The effect of randomized parameters on strength has been discussed only qualitatively.

To clarify the effect of nacreous material architecture on the failure probability distribution up to the tail probability of 10^{-6}, the connectivity of the lamellae in nacre under longitudinal tension has been simplified as a diagonally pulled fishnet with brittle links. In addition to the classical weakest-link and fiber bundle model [12–14], the fishnet turned out to be the third failure model whose probability distribution is analytically tractable [15,16]. The fishnet links were assumed to be brittle, with a steep drop after reaching the link strength. The fishnet strength distributions have been compared with those of the fiber bundle model [14,17] and of the finite weakest-link model [18–25]. Subsequently, based on the order statistics, the fishnet model was extended [26] to take into account possible gradual postpeak softening of the individual links. In that case, to determine the failure probability distribution at the peak load, it was found necessary to consider the number of damaged links at the peak load as a random variable required as an input.

A big challenge for most engineering structures, such as aircraft, bridges, or micro-electronics, is that they are supposed to be designed for failure probability less than 10^{-6} per lifetime. The tolerable load that satisfies this probability is next to impossible to determine experimentally, since about 10^8 test repetitions would be required. Therefore, a theory is needed. It must, of course, be experimentally verified by other means. The best and virtually the only means available is the size effect on the nominal strength of the structure. As already shown for calibration of the Gauss–Weibull distribution of quasi-brittle materials such as concrete, rocks, tough ceramics, fiber polymer composites, etc. [20], it suffices, for geometrically scaled specimens, to obtain the experimental data for the structure size effect on the mean strength. Here, for the sake of simplicity, instead of the sample mean strength, we consider the structure size effect on the sample median strength even though its variance is higher.

It should be noted that there are two types of size effect [20]. Type 2 [27,28] is typical for reinforced concrete. It occurs when geometrically similar large cracks develop in a stable manner prior to reaching the peak load and is also obtained in specimens with large-scaled notches. Type 2 size effect is caused by the size dependence of the release of stored strain energy. Its mean is deterministic because the crack tip location at maximum load is determined by mechanics.

Type 1 [29], which is the type considered here, occurs to structures that become unstable as soon as a macrocrack initiates from the zone of distributed damage. The macrocrack initiation can occur at many places within the random strength field, which is why the mean size effect originates from the randomness of material strength, except for the effect of stress redistribution due to finite size of the damaged zone, captured, e.g., by the finiteness of the weakest-link chain model [20] (for a broad review on quasi-brittle and fishnet failure probability, see Ref. [30]).

In the fishnet model, similar to all type 1 failures, the peak load is decided by the failure of only a few links among

[1]Corresponding author.
Contributed by the Applied Mechanics Division of ASME for publication in the JOURNAL OF APPLIED MECHANICS. Manuscript received March 26, 2019; final manuscript received April 26, 2019; published online May 23, 2019. Assoc. Editor: Yonggang Huang.

many. Thus, in a scaled-up large specimen, few links controlling the peak load can occur at many locations in the structure and, for a large enough specimen, can thus sample a broad range of failure probability distribution. This is the intuitive explanation of the fishnet size effect. Note also that, except for very large structures, the classical Weibull statistical size effect cannot be applied to nacreous and other hierarchical or architectured materials. The reason is that the one-to-one correspondence between the size effect and the strength distribution is no longer valid for materials and structures that do not behave like a chain, such as a fishnet.

Here, we first study the statistical size effect for rectangular fishnets with softening links. Instead of the exact expression, we formulate a tight upper bound on the lower tail distribution of the structural strength. We achieve it by splitting the geometrically similar scaling into longitudinal and transverse scalings and then analyze them separately. As expected, longitudinal scaling gradually transforms the structure into a chain and transverse scaling transforms the structure into a fiber bundle. Proportional combination of the two types of scaling finally gives us a size effect transitioning between a chain and a fiber bundle. Apart from the scaling relations of the mean and median, we also study those of the variance and coefficient of variation (CoV).

2 Median Versus Mean Strength

First, we try to formulate the median size effect, which describes the dependence of median structure strength on its size. It is similar to the mean size effect but is determined more easily. In the Weibull scale plot of the strength distribution, i.e., in the plot with ordinate $\ln[-\ln(1-P_f)]$ (where P_f = failure probability), the median is the point of ordinate $\ln(\ln 2)$ (for which $P_f = 0.5$).

On the other hand, even though the mean of strength could be quite hard to calculate analytically from the distribution, the mean would have practical advantages: The sample mean would converge much faster than the sample median, in the light of the law of large numbers. Therefore, one could get an accurate estimation of the true mean by a rather small number of tests. As a result, the sample mean is always preferred in testing.

To keep the advantages of both the mean and the median, we derive the size effect curve of the median, because of simplicity. But, to infer the failure probability, we treat the sample means from the tests as the medians. The effect of replacing the median strength with the mean strength in the calculations is discussed later.

3 Correspondence Between P_f and Its Median Size Effect

As mentioned in Sec. 1, the main purpose of obtaining the expression of the statistical size effect is to infer the failure probability, i.e., the strength distribution P_f. Of particular interest is the lower tail of P_f, which is almost impossible to reach with the traditional histogram testing. It is clear that for each individual strength distribution $P_f(\sigma)$, there is only one median strength $\sigma_{0.5}$ that, by definition, satisfies the condition that $P_f(\sigma_{0.5}) = 0.5$.

The reverse, however, is not necessarily true. Given a mean or median size effect curve of a structure, there may or may not be only one strength distribution that corresponds to the size effect curve. An example of multiple correspondence is the Gaussian (normal) distribution. Its variance could vary while keeping the mean fixed; therefore, knowing the mean value is not enough to fully determine the probability distribution. On the other hand, the Weibull distribution, in which the mean and the variance are fully coupled [18], is an example of one-to-one correspondence:

$$s^2 = \mu^2 \left(\frac{\Gamma\left(1+\frac{2}{m}\right)}{\Gamma^2\left(1+\frac{1}{m}\right)} - 1 \right) \tag{1}$$

where μ and s^2 are the mean and variance of the Weibull distribution, respectively, and m is the Weibull modulus. Equation 1 indicates that, given the constant m, the variance is completely fixed if the mean is known (the variance–mean coupling disappears for the three-parameter Weibull distribution, but its nonzero threshold is incorrect for strength statistics [20]).

As shown previously [15], the strength distribution of the fishnet is in the middle of the transition from the Weibull to the Gaussian distribution. Thus, it must be concluded that the correspondence between the median (mean) size effect curve and the strength distribution P_f is not one to one. Therefore, it is impossible to get the exact distribution function only from the size effect curve. Instead, to make sure the prediction would be safe for the design purposes, we seek an upper bound on P_f from the mean size effect test data.

4 Formulation of Median Statistical Size Effect

Figure 1 shows the geometries of the four fishnets used in the current study. The fishnet with a length of 128 (columns of links)

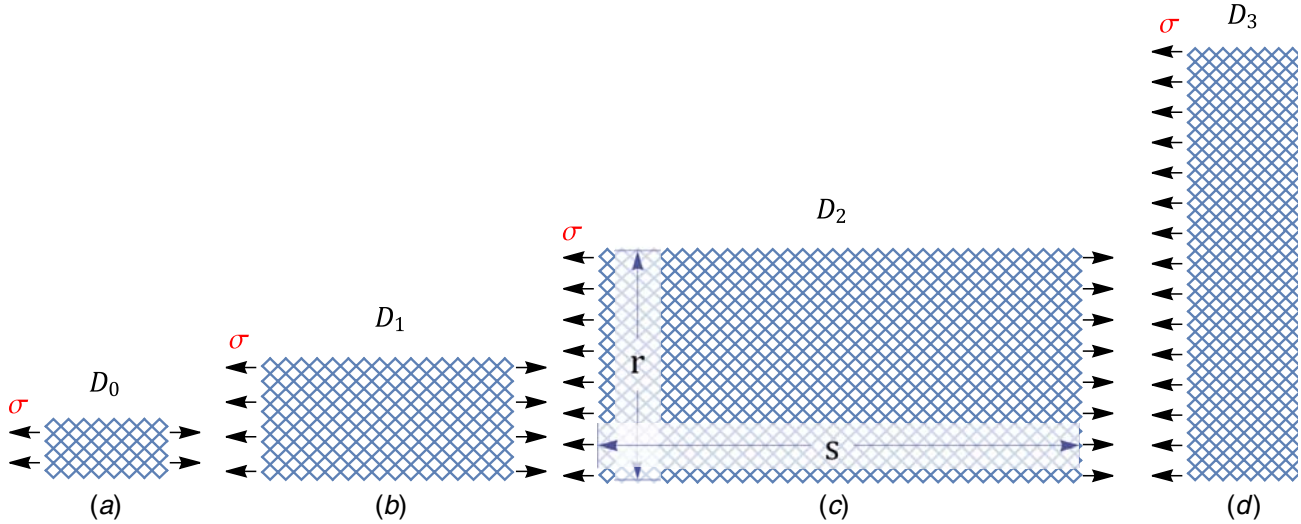

Fig. 1 Schematic showing four geometrically similar fishnets under uniaxial tension: (*a*) 8 × 16, (*b*) 16 × 32, (*c*) 32 × 64, and (*d*) 64 × 128 (partially shown). *r* and *s* denote the number of fishnet rows and columns, respectively.

and a width of 64 (rows of links) is the largest one, due partially to space limitations. For all the sizes, the aspect ratios are kept constant, as 1:2. We first study the evolution of strength distribution under longitudinal and transverse scaling. Then, the scaling of geometrically similar structures is treated as the combination of the two.

Same as previous studies [15,26], the structure of a nacreous material is simplified into a rectangular fishnet consisting of r rows and s columns of links (the rows run in the direction of tension). The mechanical behavior is similar to the so-called pantographic structures [31,32], except that we consider the truss links to be pint jointed, with no rotational stiffness. Based on the arguments in Refs. [20,22,24], the link strengths are treated as random variables that obey the grafted Gauss–Weibull distribution:

$$P_1(\sigma) = \begin{cases} 2.55\left(1 - e^{-(\sigma/12)^{10}}\right), & \sigma \le 8.6 \text{ MPa} \\ 0.53 - 0.47 \text{ erf}[0.88(10 - \sigma)], & \sigma > 8.6 \text{ MPa} \end{cases} \quad (2)$$

The link-strength distribution is here considered to be directly given, instead of being derived from a homogenized continuous random field. In other words, the autocorrelation length is set to be the same as the link length, reflecting the discrete nature of the fine-scale structure of nacreous materials. Also, by doing this, we have a direct control over the link strength distribution $P_1(\sigma)$, and its power-law tail is strictly preserved.

The fishnet links are quasi-brittle and obey a linear softening law. The brittleness of a link is characterized by the ratio $|K_t/K_0|$, where K_0 is the initial elastic stiffness of the undamaged fishnet links and K_t (<0) is the tangential softening stiffness. The steeper the softening slope, the more brittle the link. The fishnets are pulled uniaxially under displacement control. Accordingly, the nominal strength σ is measured from the boundaries: the total reaction force at peak load divided by the cross section area. Our main interest lies in the strength distribution $P_f(\sigma)$ of the whole fishnet and the size effect on its median. Figure 2 shows some of the typical numerical results, such as the stress–displacement curves and damage evolution. Since the mechanical response for each size is similar, we show the results for only one size: $r = 32$ and $s = 64$.

4.1 Longitudinal Scaling

4.1.1 Weakest-Link Behavior. To study the effect of longitudinal scaling on the strength distribution, we fix the number of rows of the fishnet at 16 ($r = 16$) and let the number of columns increase geometrically from 8 to 64 ($s = 8$, 16, 32, and 64).

The structure begins behaving more like a chain as its length increases while fixing its width. Intuitively, this implies that the limiting strength distribution of the structure is Weibullian and that long enough segments of the chain have almost independent strengths. For a long chain of n segments, each of which has a

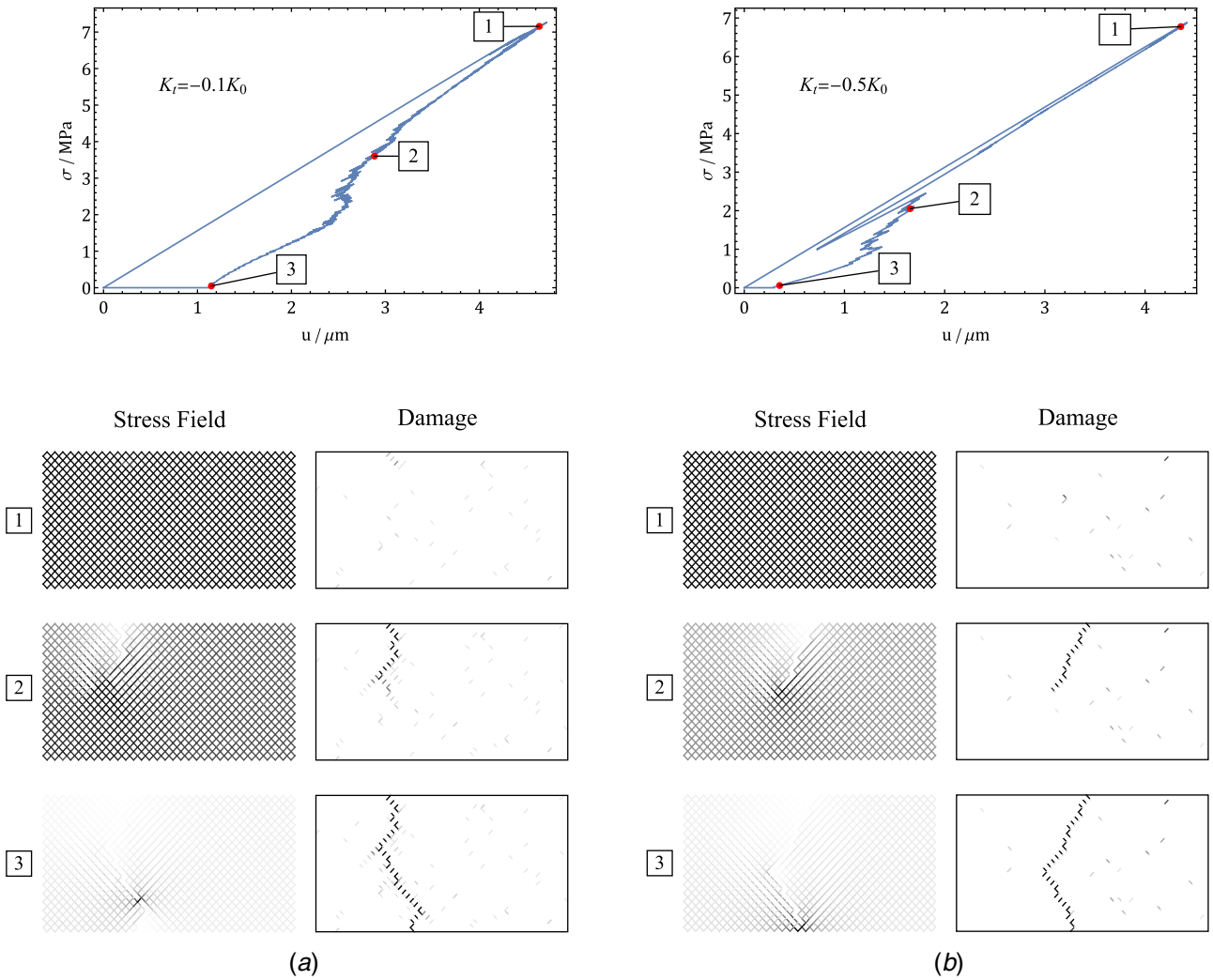

Fig. 2 Typical stress–displacement curves for fishnets of size $r \times s = 32 \times 64$ and their evolution of stress field and damage: (*a*) $K_t = -0.1K_0$ and (*b*) $K_t = -0.5K_0$ (more brittle). For each case, the number of discrete softening jumps to reach zero stress in each link $J = 20$.

survival (or strength) probability $P_s(\sigma)$, the failure probability (or strength) of the chain P_f satisfies the equation:

$$1 - P_f(\sigma) = [1 - P_s(\sigma)]^n \tag{3}$$

In other words, the survival probability of the whole chain is the joint probability of survival of all its segments (or, in other words, no segment can fail if the whole chain is safe). Taking a logarithm on both sides of Eq. (3) twice yields:

$$\ln\{-\ln[1 - P_f(\sigma)]\} = \ln[-\ln(1 - P_s(\sigma))] + \ln n \tag{4}$$

Since the ordinate and coordinate used in the Weibull scale plot (or Weibull paper) is $\ln\sigma$ and $\ln[-\ln(1 - F(\sigma))]$, respectively, the graph of P_f for the whole chain in the Weibull scale is equivalent to shifting the graph of the segment P_s upward by distance $\ln n$. This applies, of course, only for long enough fishnets, and so deviations must be expected for short fishnets.

Figure 3 shows the strength histograms obtained by Monte Carlo simulations of quasi-brittle fishnets of four different lengths (each point in these histograms represents the mean of several hundreds of fishnet finite element method simulations). It is clear that for fishnets whose lengths are greater than their width ($s > r$), the strength distributions are nearly straight lines in the Weibull scale. In addition, the vertical distance between neighboring histograms is a constant $\ln 2$, which is the logarithm of the ratio of the neighboring fishnet lengths $\ln s_2/s_1$.

These observations verify the weakest-link assumption of long fishnets. It is also observed that for the shortest fishnet with length 8, the upper and lower tail of its histogram deviate significantly from the straight line. This makes sense because this fishnet, due to its short length, is more like a fiber bundle than a chain. Similar to the chain-of-bundles model [33], this shows that the weakest-link model is a good approximation only when long enough longitudinal sections are considered as the longitudinal representative volume elements (RVEs). The model would be invalid if either short sections or single links were treated as the RVE.

It is interesting, although not surprising, that the convergence of histogram to Weibull distribution is fast in the central region close to the mean, while both the upper and lower tails converge much slower. The Weibull modulus, which represents the slope of the distribution in the Weibull scale, does not converge to the biggest value, $m = 80$, at its extreme lower tail (Fig. 3) but to an intermediate value $m = 50$. Given that the Weibull modulus of the link strengths $P_1(\sigma)$ is $m = 10$. The converged Weibull modulus is five times as large as that of a single link, which is due to the transverse coupling of links along the transverse direction. In other words, there are, on average, five damaged links for each shortest independent section prior to the maximum load. This interesting phenomenon could be related to the postpeak softening of individual links and deserves further study, which is beyond the scope of the current paper.

4.1.2 Dependence of the Median Strength on Fishnet Length. As already discussed, we try to establish a relation between the size effect curve and one corresponding upper bound on P_f. Relying on the fact that the histogram is always concave (i.e., no center of curvature lies above the histogram curve), we choose the tangent line through the median strength as the upper bound of P_f. Typically, we care about the slope near the mean or median strength, because this slope is easy to obtain from a limited number of tests. The straight lines in Fig. 3 are the tangent lines through the median strengths of each histogram. It is clear that they are the upper bounds for each corresponding distribution. Moreover, these upper bounds are Weibull distributions, which satisfy the weakest-link assumption, that is, the vertical distance between two adjacent lines is determined by the logarithm of the length ratio of the two fishnets, $\ln s_2/s_1$. Suppose the strength distribution in the Weibull scale is $Y = m\,X + C$ for the fishnet of reference length s_0, where $X = \ln\sigma$ and $Y = \ln[-\ln(1 - P_f)]$. Then, from Eq. (4), the median strength $\sigma_{0.5}$ of the fishnet with length s satisfies the following relation in the Weibull scale:

$$Y = mX + C + \ln(s/s_0), \quad \text{where } X = \ln\sigma_{0.5} \tag{5}$$

Solving for X yields:

$$\ln\sigma_{0.5} = X = -\frac{1}{m}\ln(s/s_0) + \frac{1}{m}(Y - C) \tag{6}$$

This represents the classical Weibull statistical size effect [18], where the logarithm of median (or mean) strength, $\ln\sigma_{0.5}$, depends linearly on the logarithm of normalized structure size (or length), $\ln(s/s_0)$, and the slope of the line is $-1/m$.

4.2 Transverse Scaling

4.2.1 Evolution of Histogram Under Transverse Scaling. To study the effect of transverse scaling on the strength distribution of the whole structure, we fix the number of columns of the fishnet at 16 links ($s = 16$) and let its number of rows increase in the geometric sequence from 8 to 64 ($r = 8$, 16, 32, and 64). Figure 4 shows the strength histograms obtained by Monte Carlo simulations of quasi-brittle fishnets of the four different widths.

As can be seen, the pattern of strength distributions under transverse scaling is significantly different from longitudinal scaling as shown in Fig. 3. As the fishnet becomes wider in the vertical direction (transverse to the direction of tension), the variance of the resulting strength histogram becomes smaller and the apparent

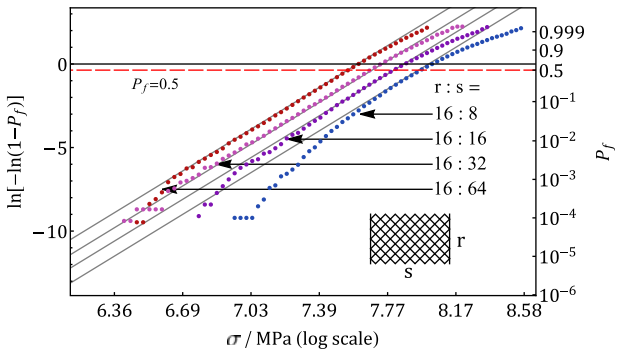

Fig. 3 Strength histogram (in the Weibull scale) of various fishnets under longitudinal scaling. The widths *r* of all fishnets are fixed at 16 rows, while their lengths *s* vary geometrically from 8 to 64 columns. For each case, the sample size is 10^4, softening slope $K_t = -0.1K_0$, and number of discrete softening jumps for each link $J = 20$.

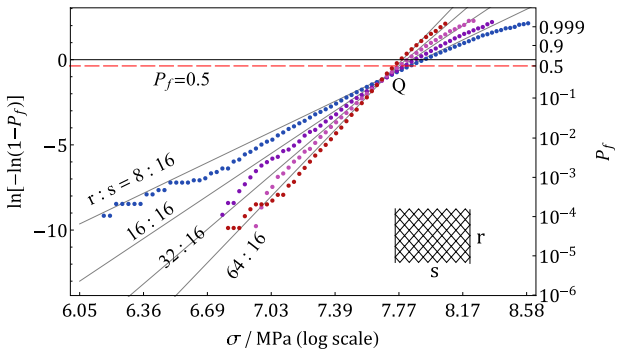

Fig. 4 Strength histogram (in the Weibull scale) of various fishnets under transverse scaling. Lengths of all fishnets, *s*, are fixed at 16, while their widths, *r*, vary in geometric sequence from 8 to 64. For each case, the sample size is 10^4, the softening slope $K_t = -0.1K_0$, and the number of discrete softening jumps to reach zero stress in each link $J = 20$.

Weibull modulus becomes larger. Because more links could fail or soften before reaching the maximum load of the whole structure. As a consequence, more survival probabilities need to be considered to formulate the strength distribution, leading to a larger slope at the lower tail.

It is striking that all the histograms intersect at almost a single point, Q, on the curve (see Fig. 4). This is explained by two observations:

(1) The upper tail region (e.g., $P_f \geq 0.9999$ or $\ln[-\ln(1-P_f)] \geq 2.22$) of the histogram always follows the weakest-link rule. Because the additional terms from the fishnet statistics do not affect the upper tail of the histogram in that the applied load is much larger than the average link strength, the neighborhood of any failed link is unlikely to survive under the redistributed stresses. The result is that the failure of any single link leads to the failure of the whole structure, same as in the weakest-link chain.
(2) Except for the upper tail, the remaining histograms are almost straight lines in the Weibull scale. The slope (Weibull modulus), m, increases as the fishnet width is scaled up in geometric sequence (see the straight line fit in Fig. 4). In addition, m grows almost linearly with $\ln r$.

With these two observations, it is now clear that, as the right end of histogram shifts up under transverse scaling, the slope also increases. Therefore, the histograms for fishnets of any two widths must intersect at a point. The reason why they intersect at a single point, Q, is that both the upward shift and the slope increase are nearly proportional to $\ln r$.

Note that the location of point Q depends on the rate of slope increase of the histogram under transverse scaling of the fishnet. The greater the rate, the higher the location of the intersection point. Meanwhile, the rate of histogram slope increase is related to the brittleness (or softening slope K_t) of the fishnet links. Therefore, the location of point Q can be seen as an indicator of the material brittleness. As the links become more brittle, the rate of slope increase gets smaller, causing the position of Q to shift further away to the lower left of the graph.

On the other hand, one can check that, as the links become more ductile, Q will be closer to the median of the distributions. The reason is that, in the limiting case of elastic-perfectly plastic links ($K_t \to 0$), the fishnets of various widths follow (in the light of the central limit theorem) the Gaussian distributions of the same mean (or median) but different variances. In that case, point Q lies exactly on the median line. Thus, the coordinate of point Q is bounded from above by the median line: $\ln[-\ln(1-P_f)] = \ln\ln 2$.

In the limiting case of $r : s \to \infty$, the strength distribution approaches that of a fiber bundle consisting of softening fibers. Again, the brittleness of the links governs the softening slope of the limiting constituent fiber. The resulting load–displacement curve is the mean curve of the responses of each single fiber. Since the number of fibers in the limiting bundle is infinite, the overall load–displacement curve is almost deterministic (converges to the mean load–displacement curve) in the light of law of large numbers, although the strength of each individual fibers are random variables.

Consequently, the bundle strength is the maximum load from the limiting deterministic load–displacement curve and the corresponding failure probability is a degenerate distribution (Heaviside step function) with finite mean and zero variance. But in this case, the limiting bundle strength is strictly smaller than the mean fiber strengths due to softening of fibers. To be more specific, we could calculate analytically the mean load–extension curves for quasi-brittle bundles. Without loss of generality, we ignore the dimensions of stress and strain (e.g., normalized by some constant stress and strain) and consider the fiber modulus to be equal to 1 (i.e., $\sigma = \epsilon$) and fiber peak load to follow the distribution $G(\sigma)$, whose density function is $g(\sigma) = G'(\sigma)$. Then, the average load–extension curve for the whole bundle is expressed as follows:

$$f(\sigma) = \int_{\sigma}^{\infty} \sigma g(\tau) d\tau + \int_{\eta\sigma}^{\sigma} \left(\tau + (\sigma - \tau)\frac{K_t}{K_0}\right) g(\tau) d\tau \tag{7}$$

where

$$\eta = \frac{K_t}{K_t - K_0} \tag{8}$$

The first integral in Eq. (7) reduces to $\sigma[1 - G(\sigma)]$, which is the mean load–displacement curve for brittle bundles, as shown by Daniels [14] in 1945. It only accounts for the situation where fibers survive under load σ (as brittle fibers directly fail after strength is reached). The second integral in Eq. (7) considers the case where fibers are softened but still not completely failed and thus contributes to the bundle strength. The lower bound of the second integral is $\eta\sigma$ rather than 0, because the residual strength of the softened fiber is $\tau + (\sigma - \tau)K_t/K_0$, which is greater than zero when $\tau > \eta\sigma$. Otherwise, the fiber has failed completely, contributing no load. Note that if $K_t \to -\infty$ (perfectly brittle fibers), the value of η approaches 1, making the second integral in Eq. (7) vanish. Then, the result reduces to the brittle case studied by Daniels.

Figure 5 shows the comparison of average load–extension curves of bundles with three different brittleness levels. It is clear that as constituent fibers become more brittle, the peak load decreases.

As the other extreme case, in which the links are perfectly elastic–plastic, i.e., a ductile bundle, the law of large numbers directly applies to the bundle strength, while in the previous case, it only applied to the entire load–displacement curve. Therefore, the bundle strength is not only a constant but also is exactly the same as the mean fiber strength.

To conclude, for extremely wide fishnets, for which $r : s \to \infty$, their points of rotation Q are all very close to the median line $y_0 = \ln\ln 2$, but their horizontal positions x_0 vary due to different post-peak softening slopes of the fibers and are bounded by the mean fiber (or link) strength $\bar{\sigma}$, i.e., $x_0 \leq \ln\bar{\sigma}$, which is an equality that holds for perfectly ductile bundles.

4.2.2 Dependence of the Median Strength on Fishnet Width. Now that we have clarified how the histograms evolve under transverse scaling of the fishnet width, we can obtain the relation between the median strength and the fishnet width. Let the coordinates of the intersection point Q be (x_0, y_0). Then, the family of Weibull approximations of the true strength distributions under transverse scaling can be expressed as follows:

$$Y - y_0 = m(r)(X - x_0) \tag{9}$$

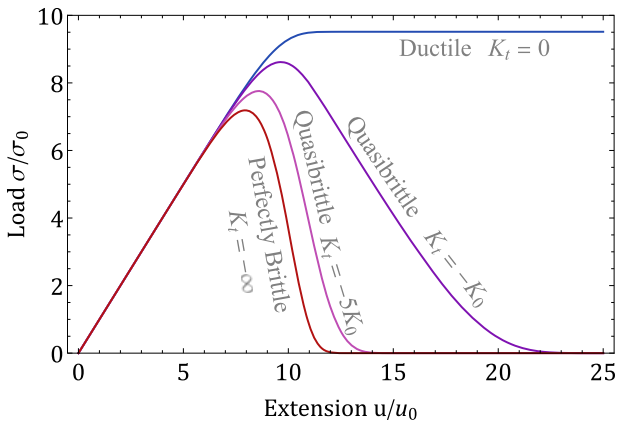

Fig. 5 Comparison plot of analytical results of mean load–extension curves of bundles with different fiber brittleness. Fiber strengths are i.i.d. random variables and follow the same distribution $G(\sigma)$ for all three cases.

where $m(r)$ is the apparent Weibull modulus which, for simplicity, is assumed to depend linearly on ln r:

$$m(r) = m_0[1 + c \ln (r/r_0)] \tag{10}$$

Here, m_0 is the Weibull modulus for the reference fishnet width and c is the rate of slope (or Weibull modulus) increase. Combining Eqs. (9) and (10) and plugging in $Y = \ln(\ln 2)$, one can solve for the median strength, $X = \sigma_{0.5}$:

$$\ln \sigma_{0.5} = \frac{\ln (\ln 2) - y_0}{m_0[1 + c \ln (r/r_0)]} + x_0 \tag{11}$$

4.3 Statistical Median Size Effect. As discussed earlier, the scaling of geometrically similar structures is treated as the combination of longitudinal and transverse scaling in a proportional fashion. To make sure that the scaling is geometrically similar and the aspect ratio is a constant, the scaling of fishnet length and width must be done at the same rate:

$$s = Ds_0 \quad \text{and} \quad r = Dr_0 \tag{12}$$

where $D > 1$ is the dimensionless size. Combining the effect of longitudinal (Eq. (6)) and transverse (Eq. (11)) scaling on the strength distribution gives the following equation:

$$Y - y_0 = m_0[1 + c \ln (r/r_0)](X - x_0) + \ln (s/s_0) \tag{13}$$

Here, the first term on the right-hand side of the equation is the same as the expression for transverse scaling (Eq. (9)). The second term takes into account the longitudinal (chain) scaling (Eq. (5)). Finally, we replace r/r_0 and s/s_0 by the dimensionless size D and set $P_f = 0.5$ or equivalently $Y = \ln \ln 2$. Solving for X yields:

$$\ln \sigma_{0.5} = X = \frac{\ln \ln 2 - y_0 - \ln D}{m_0(1 + c \ln D)} + x_0 \tag{14}$$

Equation (14) is the median size effect relation that describes the relation between the logarithms of the median strength X and the dimensionless size D. There are four parameters in this relation; they are as follows: x_0, y_0, c, and m_0, where (x_0, y_0) is the coordinate of the point of rotation, Q, under transverse scaling; c is the rate of slope increase for histograms under transverse scaling; and m_0 is the apparent Weibull modulus for the reference size fishnet. Note that m_0 is generally not the same as the Weibull modulus of the link strength distribution and depends on the shape of the chosen reference size fishnet.

5 Inference of P_f from Size Effect

The ultimate goal of obtaining the size effect curve (Eq. (14)) is to infer the upper bound on the failure probability distribution (or the strength distribution) of the whole structure for various sizes. This is achieved by substituting into Eq. (13) the parameters obtained from the size effect curve:

$$Y = \ln [-\ln (1 - P_f)] = m_0(1 + c \ln D)(X - x_0) + y_0 + \ln D \tag{15}$$

Solving for $P_f(\sigma)$ and using the fact that $X = \ln \sigma$ yields the upper bound (i.e., Weibull) estimation of the strength distribution:

$$P_f(\sigma) = 1 - \exp\left\{-n\left(\frac{\sigma}{\sigma_0}\right)^m\right\} \tag{16}$$

where $n = De^{y_0}$, $\sigma_0 = e^{x_0}$, and $m = m_0(1 + c \ln D)$.

Figures 6 and 7 show the histograms of fishnet strength for various sizes. It is a common feature that both the mean and the variance of strength decrease as the fishnet size increases. In addition, the variances for the more ductile case ($K_t = -0.1K_0$) are much smaller than those for the more brittle case ($K_t = -0.5K_0$).

To illustrate the mean or median size effect, Fig. 8 shows the median size effect curves using the median strengths of the samples obtained from the histograms of the Monte Carlo simulations in Figs. 6 and 7. The optimum fit of the data by Eq. (14) is also shown for comparison. It is clear that the size effect relation is monotonically decreasing and has a convex curvature, which is a

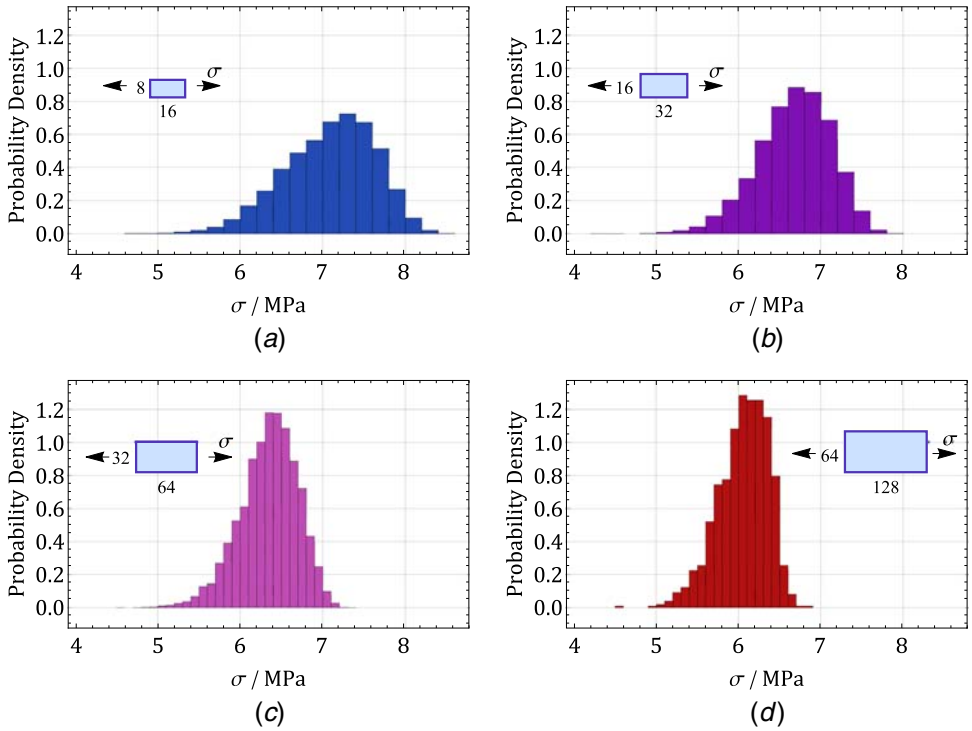

Fig. 6 Strength histograms of fishnets ($K_t = -0.5K_0$) of four typical sizes under uniaxial tension: (*a*) 8 × 16, (*b*) 16 × 32, (c) 32 × 64, and (*d*) 64 × 128. The counts have been normalized to probability density.

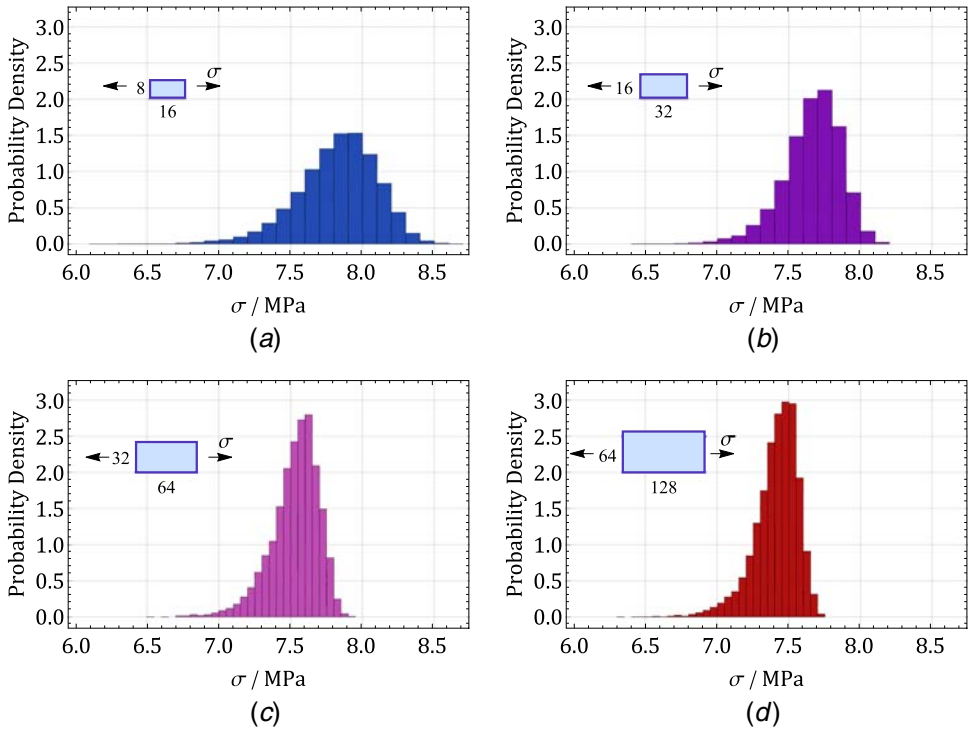

Fig. 7 Strength histograms of fishnets ($K_t = -0.1K_0$) of four typical sizes under uniaxial tension: (*a*) 8 × 16, (*b*) 16 × 32, (c) 32 × 64, and (*d*) 64 × 128. The counts have been normalized to probability density.

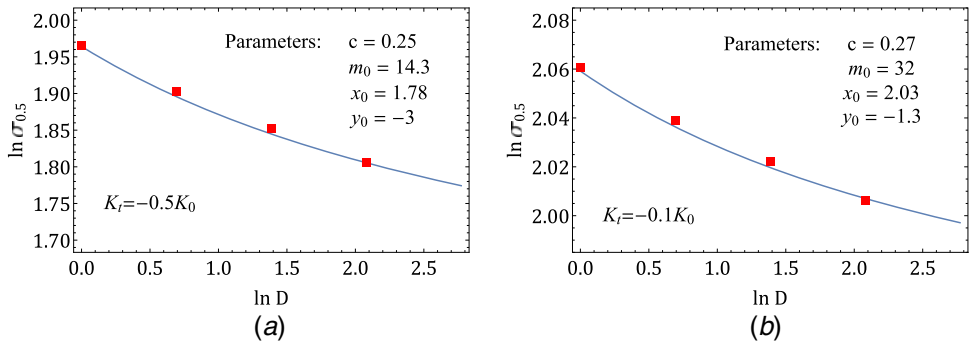

Fig. 8 Optimum fit of the size effect relation (ln $\sigma_{0.5}$ versus ln D) using the sample median strength obtained from Monte Carlo simulations. Two different brittleness levels given by $K_t = -0.5K_0$ and $-0.1K_0$ are considered here. The data points are the sample median strengths for the four typical sizes, and the curve is the optimum fit.

general feature of the type 1 size effect [19,20]. As discussed earlier, parameters c and y_0 indicate the brittleness of the fishnet links. By comparing the parameters of the optimum fit in Figs. 8(*a*) and 8(*b*), we see that the rate of slope increase under transverse scaling, c, increased from 0.25 to 0.27, as the links became less brittle. Meanwhile, the distance between Q and the median line, $y_0 - \ln \ln 2$, decreased from 2.63 to 0.93: the more ductile the material, the closer it is to the median line for Q.

By using the optimal parameters, one obtains the predictions of the upper bound failure probability for the fishnet. The predictions and actual histograms are shown, for comparison, in the Weibull scale in Fig. 9. In general, the predictions match the histograms pretty well in the regions near and above the mean strength. Since the curve of the actual failure probability keeps bending downward as the slope keeps increasing while moving toward the lower tail, it is no surprise that the histograms starts to deviate from the Weibull upper bound, which is a straight line.

Note that all the predictions intersect at a single point. An interesting consequence of this is that, below the point of intersection, the structure strength might increase as the size increases, which is exactly the opposite of the trend at the mean level. Whether this reverse trend would actually happen in the probability range that we are interested in ($10^{-7} \le P_f \le 10^{-5}$) depends on the brittleness of the material. This indicates that, even though the structure becomes weaker as it becomes larger, in the sense that the mean strength decreases, it could become stronger at the level of $P_f = 10^{-6}$ in the lower tail of failure probability. In other words, a reverse size effect can occur at the tail of failure probability level.

Finally, due to a much faster convergence rate, one could also use the mean strengths from the test data to replace the median strengths used in the current model.

This will lead to a safer (less tight) upper bound compared with using the median. The reason is that, for the Weibull distribution of modulus $m > 3.44$, the median is slightly greater than the mean

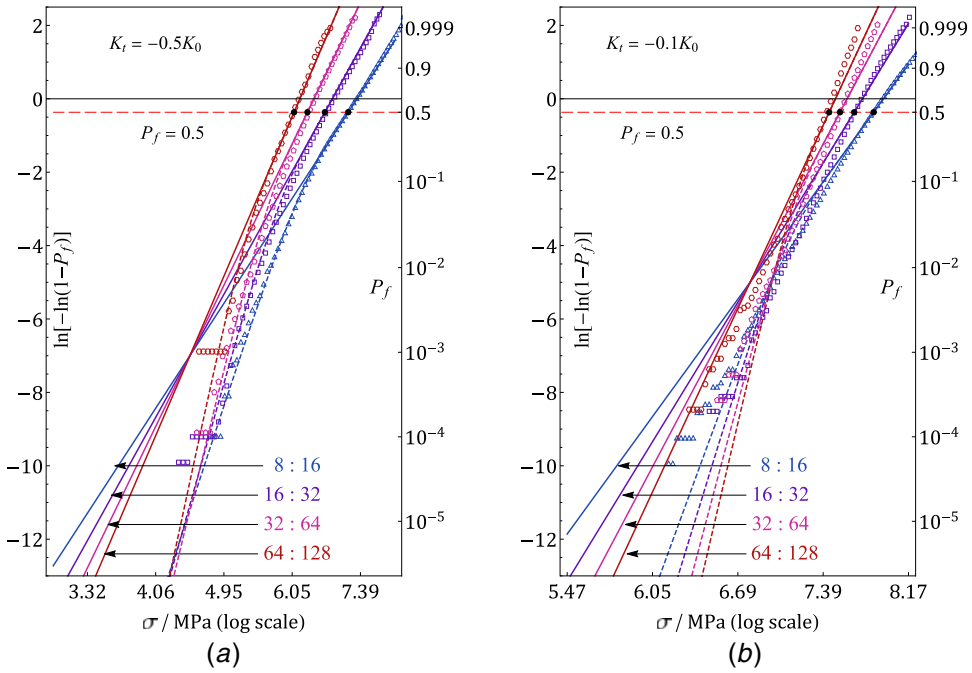

Fig. 9 Comparison of predicted (thick lines) upper bound strength distributions of the fishnet with the actual histograms (discrete markers). Optimum fit by the homogenized two-term fishnet model is shown by dashed curves.

(precisely, the mean $= \sigma_0\Gamma(1 + 1/m)$ and the median $= \sigma_0\ (\ln 2)^{1/m}$). On the other hand, for symmetric distributions such as the Gaussian, the mean is exactly equal to the median. Since general strength distributions of fishnets lie between those of Weibull and Gaussian distributions, their medians are slightly larger than their mean values. This fact, which is the consequence of negative skewness of the Weibull and related fishnet distributions, means that the substitution of a mean for the median predicts the safety to be slightly higher than it actually is.

6 Homogenization of Fishnet Statistics

Noting that the actual strength histogram deviates downward from our upper bound prediction and bends down more in the lower tail, we may naturally ask whether there exists a general model that could capture this phenomenon. For this purpose, we resort to the two-term fishnet model with a homogenized (equivalent) link strength distribution $\tilde{P}_1(\sigma)$.

First, we start with the upper bound prediction, Eq. (16), which is the Weibull distribution obtained in Sec. 5 and is denoted as $P_{f_0}(\sigma)$. The predicted Weibull modulus m in $P_{f_0}(\sigma)$ is larger than the value for a single link m_0. The ratio m/m_0 indicates the size of the equivalent course-grained "link." Therefore, the total number of equivalent "links" is $N_{\text{eq}} = r\,s/(m/m_0)$. Then, $\tilde{P}_1(\sigma)$ is calculated by reverse scaling from $P_{f_0}(\sigma)$ for the equivalent chain back to a single link:

$$\tilde{P}_1(\sigma) = 1 - [1 - P_{f_0}(\sigma)]^{1/N_{\text{eq}}} \tag{17}$$

Finally, we apply the two-term fishnet model to the coarse-grained system:

$$P_f(\sigma) = P_{f_0}(\sigma) - N_{\text{eq}}\tilde{P}_1(\sigma)[1 - \tilde{P}_1(\sigma)]^{N_{\text{eq}}-\nu-1}[1 - \tilde{P}_1(\eta\sigma)]^{\nu} \tag{18}$$

where ν is the equivalent size of the stress redistribution region and η is the equivalent stress redistribution factor.

The dashed curves in Fig. 9 show the optimum fit of the histogram data given by Eq. (18). The homogenized two-term fishnet model shows the ability to capture the lower tail behavior of the strength histograms of fishnets with various sizes. However, this improvement does not come without a price. The model requires more information apart from the mean (or median) size effect. More specifically, one must know the value of m_0 in $P_1(\sigma)$, ν, and η a priori, while the upper bound prediction (Eq. (16)) only requires the size effect relation, which is much easier to obtain by tests.

7 Scaling Relations for Variance and CoV of Strength

Apart from the scaling relations for the mean and median values of the strength distributions, the size effect on the variance and CoV is also critical to characterize the reliability of a structure. One would expect that the scaling relations for variance and CoV (the standard deviation divided by the mean) should depend heavily on the brittleness of the material characterized by K_t: if the material is ductile (very low $|K_t|$), the scaling law of variance is dictated by the central limit theorem, as for the ductile fiber bundle; on the other hand, if the material is brittle (very high $|K_t|$), the variance should have a different scaling relation and is mainly governed by the weakest-link rule. Therefore, we first examine the foregoing two limiting cases. Then, the cases where the fishnet links exhibit gradual postpeak softening (medium $|K_t|$) should lie between the two extreme cases.

For the weakest-link model consisting of n links, the strength distribution is

$$P_f(\sigma) = 1 - e^{-n(\sigma/\sigma_0)^m} = 1 - \exp\left(\frac{\sigma}{n^{-1/m}\sigma_0}\right)^m \tag{19}$$

Based on this cumulative distribution function (CDF), we could calculate its variance:

$$\text{Var} = (n^{-1/m}\sigma_0)^2\left[\Gamma\left(1 + \frac{2}{m}\right) - \Gamma^2\left(1 + \frac{1}{m}\right)\right] \propto n^{-2/m} \tag{20}$$

Since, for two-dimensional scaling, $n = \alpha D^2$, we have

$$\text{Var} \propto D^{-4/m} \tag{21}$$

From Eq. (1), the CoV of Weibull distributions is a constant, that is, independent of n.

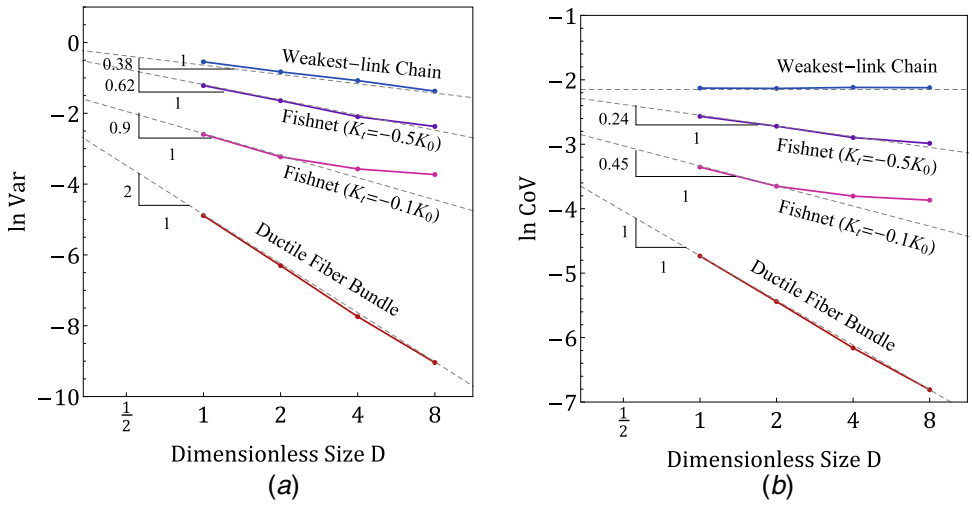

Fig. 10 Two-dimensional geometrically similar scaling relations of (*a*) variance and (*b*) CoV for the weakest-link chain (brittle limit), fishnets, and the ductile fiber bundle (ductile limit). Weibull modulus for the strength distribution, $P_1(\sigma)$, of links is $m = 10$.

For the ductile case, the structural limit is a ductile bundle of n fibers. From the central limit theorem, the variance, Var, scales as n^{-1}. Since $n = \alpha D^2$, we have

$$\text{Var} \propto D^{-2} \tag{22}$$

In addition, the sample mean does not change with n; therefore, the CoV scales as $\sqrt{\text{Var}}$, that is, $\text{CoV} \propto D^{-1}$.

To sum up, we show the scaling relations of variance and CoV for the brittle and ductile limits in the following table:

	Var	CoV
Brittle	$D^{-4/m}$	Constant
Ductile	D^{-2}	D^{-1}

Figure 10 shows the measured scaling relations of variance and CoV as functions of the dimensionless size $D = r/r_0 = s/s_0$ in log scale. Here, the size of the smallest fishnet ($r_0 = 8$, $s_0 = 16$) is chosen as the reference size. The brittle and ductile limit of the scaling relations of variance and CoV match very well with the analytical expressions (Eqs. (21) and (22)). The slope measured for the variance of the weakest-link model is −0.38, which is slightly greater than the value predicted by the theory ($-4/m = -0.4$). This small discrepancy is due to the fact that $P_1(\sigma)$ is not completely a Weibull distribution but only that it has a Weibull lower tail.

From both figures, it is clear that the variance and CoV of the fishnet strength distribution lie in the middle of the two limits, and as fishnet links become more brittle, the variance and the CoV tend to those of the chain. As the links become more ductile, the behavior of variance and CoV is more similar to the ductile bundle. As expected, the scaling relations of variance and CoV of the strength distributions for general fishnets depend on the brittleness of the links. They transit continuously from that of a brittle chain to that of a ductile bundle.

Interestingly, the CoV of the more ductile fishnet ($K_t = -0.1K_0$) gradually tends to a constant very fast (see Fig. 10(*b*)). This is because, under longitudinal scaling, the overall response of the fishnet becomes more brittle, making its strength distribution converge to a Weibull distribution. As a result, the evolution of CoV tends to a constant for the large-size limit. Similar behavior is also seen for the more brittle fishnet, but if the fishnet is already more brittle and has a relatively small CoV, this phenomenon is not as significant.

8 Conclusions

(1) The statistical median size effect relation for nacreous biomimetic materials is not difficult to derive. But an analytical mean size effect relation appears to be much more difficult to obtain.
(2) An effective way to obtain the size effect relation is to analyze first longitudinal and transverse (or lateral) scalings separately, and then superpose the results to obtain the two-dimensional scaling.
(3) In view of the negative skewness of all the distributions, replacing the mean by the median yields a safe bound on the failure probability at any given stress, i.e., give a conservative result.
(4) The longitudinal scaling leads to a vertical upward shift of the distribution in the Weibull scale, while the transverse scaling leads to a counterclockwise rotation of the distribution about a fixed point located below the median.
(5) Because of the rotation of the failure probability distribution at transverse scaling, a reverse size effect at two-dimensional scaling may take place, i.e., a trend opposite to the mean size effect may occur: The strength at which $P_f = 10^{-6}$ may increase as the structure size increases. This is, of course, advantageous for design safety.
(6) An upper bound, i.e., safe, estimate for the tail of the failure probability of nacreous materials of any size and shape can be inferred from the calibrated parameters of the size effect relation.
(7) Unlike histogram testing, the size effect method of estimating a tight upper bound on the failure probability distribution requires only about six tests for each of several scaled fishnet sizes.
(8) Millions of Monte Carlo simulations confirm the analytical results.
(9) The inference method developed here is applicable to nacreous materials whose links have any postpeak softening properties, i.e., brittle, quasi-brittle, or almost elastic–perfectly plastic.

Funding Data

- ARO Grant No. W91INF-19-1-0039 to Northwestern University

References

[1] Wang, R. Z., Suo, Z., Evans, A. G., Yao, N., and Aksay, I. A., 2001, "Deformation Mechanisms in Nacre," J. Mater. Res., **16**(9), pp. 2485–2493.

[2] Wei, X., Filleter, T., and Espinosa, H. D., 2015, "Statistical Shear Lag Model—Unraveling the Size Effect in Hierarchical Composites," Acta Biomater., **18**, pp. 206–212.

[3] Verho, T., Karppinen, P., Gröschel, A. H., and Ikkala, O., 2018, "Imaging Inelastic Fracture Processes in Biomimetic Nanocomposites and Nacre by Laser Speckle for Better Toughness," Adv. Sci., **5**(1), p. 1700635.

[4] Kamat, S., Su, X., Ballarini, R., and Heuer, A. H., 2000, "Structural Basis for the Fracture Toughness of the Shell of the Conch Strombus Gigas," Nature, **405**(6790), p. 1036.

[5] Williamson, D. M., and Proud, W. G., 2011, "The Conch Shell as a Model for Tougher Composites," Int. J. Mater. Eng. Innovat., **2**(2), pp. 149–164.

[6] Zaheri, A., Fenner, J. S., Russell, B. P., Restrepo, D., Daly, M., Wang, D., Hayashi, C., Meyers, M. A., Zavattieri, P. D., and Espinosa, H. D., 2018, "Revealing the Mechanics of Helicoidal Composites through Additive Manufacturing and Beetle Developmental Stage Analysis," Adv. Funct. Mater., **28**(33), p. 1803073.

[7] Rosewitz, J. A., Choshali, H. A., and Rahbar, N., 2019, "Bioinspired Design of Architected Cement-Polymer Composites," Cem. Concr. Compos., **96**, pp. 252–265.

[8] Huang, T.-H., Chen, C.-S., and Chang, S.-W., 2018, "Microcrack Patterns Control the Mechanical Strength in the Biocomposites," Mater. Des., **140**, pp. 505–515.

[9] Wu, K., Zheng, Z., Zhang, S., He, L., Yao, H., Gong, X., and Ni, Y., 2019, "Interfacial Strength-Controlled Energy Dissipation Mechanism and Optimization in Impact-Resistant Nacreous Structure," Mater. Des., **163**, p. 107532.

[10] Nukala, P. K. V. V., and Simunovic, S., 2005, "A Continuous Damage Random Thresholds Model for Simulating the Fracture Behavior of Nacre," Biomaterials, **26**(30), pp. 6087–6098.

[11] Abid, N., Mirkhalaf, M., and Barthelat, F., 2018, "Discrete-Element Modeling of Nacre-Like Materials: Effects of Random Microstructures on Strain Localization and Mechanical Performance," J. Mech. Phys. Solids, **112**, pp. 385–402.

[12] Weibull, W., 1939, "The Phenomenon of Rupture in Solids," Proc. Royal Swedish Inst. Eng. Res., **153**, pp. 1–55.

[13] Fisher, R. A., and Tippett, L. H. C., 1928, "Limiting Forms of the Frequency Distribution of the Largest or Smallest Member of a Sample," Math. Proc. Cambridge Philos. Soc., **24**(2), pp. 180–190.

[14] Daniels, H. E., 1945, "The Statistical Theory of the Strength of Bundles of Threads. I," Proc. Roy. Soc. Lond. Math. Phys. Soc., **183**(995), pp. 405–435.

[15] Luo, W., and Bažant, Z. P., 2017, "Fishnet Statistics for Probabilistic Strength and Scaling of Nacreous Imbricated Lamellar Materials," J. Mech. Phys. Solids, **109**, pp. 264–287.

[16] Luo, W., and Bažant, Z. P., 2017, "Fishnet Model for Failure Probability Tail of Nacre-Like Imbricated Lamellar Materials," Proc. Natl. Acad. Sci. USA, **114**(49), pp. 12900–12905.

[17] Salviato, M., and Bažant, Z. P., 2014, "The Asymptotic Stochastic Strength of Bundles of Elements Exhibiting General Stress–Strain Laws," Probabilist. Eng. Mech., **36**, pp. 1–7.

[18] Bažant, Z. P., and Planas, J., 1997, *Fracture and Size Effect in Concrete and Other Quasibrittle Materials*, Vol. 16. CRC Press, Boca Raton, FL.

[19] Bažant, Z. P., 2005, *Scaling of Structural Strength*, Elsevier, London.

[20] Bažant, Z. P., and Le, J.-L., 2017, *Probabilistic Mechanics of Quasibrittle Structures: Strength, Lifetime, and Size Effect*, Cambridge University Press, Cambridge, UK.

[21] Bažant, Z. P., Le, J.-L., and Bažant, M. Z., 2009, "Scaling of Strength and Lifetime Probability Distributions of Quasibrittle Structures based on Atomistic Fracture Mechanics," Proc. Natl. Acad. Sci. USA, **106**(28), pp. 11484–11489.

[22] Bažant, Z. P., and Pang, S.-D., 2007, "Activation Energy Based Extreme Value Statistics and Size Effect in Brittle and Quasibrittle Fracture," J. Mech. Phys. Solids, **55**(1), pp. 91–131.

[23] Le, J. L., and Bažant, Z. P., 2009, "Finite Weakest Link Model With Zero Threshold for Strength Distribution of Dental Restorative Ceramics," Dent. Mater, **25**(5), pp. 641–648.

[24] Le, J.-L., Bažant, Z. P., and Bažant, M. Z., 2011, "Unified Nano-Mechanics Based Probabilistic Theory of Quasibrittle and Brittle Structures: I. Strength, Static Crack Growth, Lifetime and Scaling," J. Mech. Phys. Solids, **59**(7), pp. 1291–1321.

[25] Le, J.-L., Ballarini, R., and Zhu, Z., 2015, "Modeling of Probabilistic Failure of Polycrystalline Silicon Mems Structures," J. Am. Ceram. Soc., **98**(6), pp. 1685–1697.

[26] Luo, W., and Bažant, Z. P., 2018, "Fishnet Model With Order Statistics for Tail Probability of Failure of Nacreous Biomimetic Materials With Softening Interlaminar Links," J. Mech. Phys. Solids, **121**, pp. 281–295.

[27] Bažant, Z. P., 1984, "Size Effect in Blunt Fracture: Concrete, Rock, Metal," J. Eng. Mech., **110**(4), pp. 518–535.

[28] Bažant, Z. P., and Kazemi, M. T., 1990, "Determination of Fracture Energy, Process Zone Longth and Brittleness Number From Size Effect, With Application to Rock and Conerete," Int. J. Fracture, **44**(2), pp. 111–131.

[29] Bažant, Z. P., and Li, Z., 1995, "Modulus of Rupture: Size Effect Due to Fracture Initiation in Boundary Layer," J. Struct. Eng., **121**(4), pp. 739–746.

[30] Bažant, Z. P., 2019, "Design of Quasibrittle Materials and Structures to Optimize Strength and Scaling at Probability Tail: An Apercu," Proc. R. Soc. A, **475**(2224), p. 20180617.

[31] Turco, E., Dell'Isola, F., Cazzani, A., and Rizzi, N. L., 2016, "Hencky-Type Discrete Model for Pantographic Structures: Numerical Comparison With Second Gradient Continuum Models," Z. Angew. Math. Phys., **67**(4), p. 85.

[32] Boutin, C., Dell'Isola, F., Giorgio, I., and Placidi, L., 2017, "Linear Pantographic Sheets: Asymptotic Micro-Macro Models Identification," Math. Mech. Complex Syst., **5**(2), pp. 127–162.

[33] Harlow, D. G., and Phoenix, S. L., 1978, "The Chain-of-Bundles Probability Model for the Strength of Fibrous Materials I: Analysis and Conjectures," J. Compos. Mater., **12**(2), pp. 195–214.